Optics Letters

Few-cycle optical pulse characterization under phase-mismatching

Yunlong Mo,[1] Wei Cao,[1,*] Huiyao Xu,[1] Kang Mi,[1] Xuechun Sun,[1] Qingbin Zhang,[1] and Peixiang Lu[1,2,3]

[1]School of Physics and Wuhan National Laboratory for Optoelectronics, Huazhong University of Science and Technology, Wuhan 430074, China
[2]Hubei Key Laboratory of Optical Information and Pattern Recognition, Wuhan Institute of Technology, Wuhan 430205, China
[3]e-mail: lupeixiang@mail.hust.edu.cn
*Corresponding author: weicao@hust.edu.cn

Received 8 December 2020; revised 30 December 2020; accepted 6 January 2021; posted 6 January 2021 (Doc. ID 417098); published 22 January 2021

The phase-matching bandwidth of nonlinear crystal is of great significance in ultrashort laser pulse characterization. In order to satisfy the phase-matching bandwidth, ultrathin nonlinear crystals are generally required. However, the significantly reduced conversion efficiency, as well as the machining difficulties, limits its applications. Here, we show that sufficient spectrum bandwidth response can be achieved for a thick crystal when the phase-matching wavelength is tuned outside of the spectral window of the measured pulse. By applying this phenomenon to a single-shot second-harmonic generation frequency resolved optical gating (SHG-FROG) device, we successfully characterized a few-cycle pulse using a 150 μm β-barium borate (BBO) crystal. The accuracy of the method was verified by comparing the conventional pulse retrieving approach with a 5 μm BBO crystal, which has a sufficient phase-matching bandwidth.

https://doi.org/10.1364/OL.417098

With the development of the ultrafast laser technique, laser pulses that contain only a few optical cycles become routinely available [1–7], leading to the emergence of strong field physics, attosecond physics, and attosecond chemistry [8–12]. The temporal waveform of the short pulses is the key for the relevant applications and, thus, the ability to implement a complete diagnosis of the pulse, i.e., obtain both its phase and amplitude information, becomes particularly important.

There are many well-established methods for measuring ultrashort laser pulses at present, the simplest of which is nonlinear intensity autocorrelation [13,14]. However, intensity autocorrelation only can access the time domain intensity profile of the ultrashort pulse, missing the phase information. Improved approaches including frequency resolved optical gating (FROG) [15–17], spectral phase interferometry for direct electric field reconstruction (SPIDER) [18,19], and dispersion scan (D-scan) [20,21] have been developed. Complete characterization of a given pulse can be carried out using an iterative algorithm in FROG [22–24] and D-scan [25]. The advantage of SPIDER is that it is easier to extract the phase from SPIDER trace than FROG and D-scan; however, the setup is more intricate [26]. For all the methods mentioned, if only partial frequency components of a broadband pulse are phase-matched, then the retrieving process could be problematic, leading to inaccurate or even erroneous results [27]. Therefore, it is a general prerequisite that the phase-matching bandwidth has to be sufficiently large in order to achieve reliable measurement for pulses bearing broad bandwidth.

Ultra-thin nonlinear crystals are used to address the bandwidth requirement for ultrashort pulses [28]. However, it suffers relatively low efficiency and machining difficulties [29]. Scheme measuring ultrashort laser pulses to achieve broad phase-matching bandwidth using thick nonlinear crystals has been reported [30]. A complete second-harmonic spectrum is measured by rotating the angle of a thick BBO continuously to match different wavelengths during the spectrometer exposure time. Although this scheme improves the efficiency of the second harmonic to a great extent, the intensity normalization of each step is relatively rigorous in the measurement process, and the whole measurement process is time-consuming. Recently, a new *in situ* method of ultrashort pulse measurement has been developed using two-dimensional materials [31], which is completely independent of the phase-matching bandwidth. However, this scheme is limited by the wavelength-dependent nonlinear polarimetry and second-harmonic efficiency of two-dimensional materials.

In this Letter, we present an efficient and reliable method that allows retrieval of the phase of a broadband laser pulse using a thick nonlinear crystal. It shows that when the phase-matching wavelength of a thick nonlinear crystal is tuned outside of the spectral window of the measured pulse, a sufficient spectrum bandwidth response can be obtained. By applying such configuration to a second-harmonic generation (SHG)-FROG device, a FROG trace without losing spectral width can be obtained. Numerical simulations show that the phase of a broadband pulse can be accurately measured using a standard retrieving algorithm. Experimentally, we demonstrate the successful measurement of an 8.6 fs few-cycle laser pulse using a 150 μm thick barium borate (BBO) crystal. The measured results are consistent with that using a 5 μm BBO crystal that supports

sufficient phase-matching bandwidth, proving the validity of the current method.

For a few-cycle pulse, its FROG trace is easily affected by linear and nonlinear factors in the measurement process due to its broad spectral bandwidth. Baltuska *et al*. have shown that the measured FROG trace can be described as a product of the spectral filtering function and the ideal FROG trace [28]:

$$S_{\text{meas}}(\Omega, \tau, \theta, L) \propto R(\Omega, \theta) S_{\text{FROG}}^{\text{SHG}}(\Omega, \tau), \tag{1}$$

where

$$S_{\text{FROG}}^{\text{SHG}}(\Omega, \tau) = \left| \int \tilde{\varepsilon}(\Omega - \omega)\tilde{\varepsilon}(\omega)\exp(i\omega\tau)\mathrm{d}\omega \right|^2, \tag{2}$$

where Ω and ω are angular frequency of the second harmonic and fundamental light, respectively. S_{meas} represents the real measured trace. R donates spectral filtering function, while θ is the phase-matching angle of the nonlinear crystal. $S_{\text{FROG}}^{\text{SHG}}$ is the ideal FROG trace, and τ is the delay between the few-cycle pulse and its replica. L is the thickness of the nonlinear crystal. $\tilde{\varepsilon}(\omega)$ expresses Fourier transform of the fundamental light. In order to extract the correct phase information of the few-cycle pulse, it is essential to divide the measured FROG trace by the spectral filtering function $R(\Omega, \theta)$ to obtain the ideal FROG trace for pulse reconstruction. The spectral filtering function is described as [28]

$$R(\Omega, \theta) = Q(\Omega)\frac{\Omega^3}{n_E(\Omega,\theta)}[(n_E^2(\Omega, \theta) - 1)(n_o^2(\Omega/2) - 1)^2]^2 \times \text{sinc}^2\left(\frac{\Delta k(\Omega/2, \Omega/2, \theta)L}{2}\right). \tag{3}$$

$Q(\Omega)$ describes the linear spectral response of the optical components and spectrometer. The terms in brackets depict the dispersion of the nonlinear susceptibility. sinc^2 term represents the phase-matching efficiency. Due to the complexity of measuring $R(\Omega, \theta)$ in experiment, it is an alternative to use the ratio between the auto-convolution of the measured spectrum by spectrometer and the FROG trace frequency marginal to represent $R(\Omega, \theta)$ [29,32,33].

Figure 1 shows the second-harmonic spectrum of an 8 fs 730 nm Gaussian ultrashort laser pulse, calculated by Eqs. (1)–(3) ($\tau = 0$), as a function of the thickness of the BBO crystal for different phase-matching angles. The phase-matching angle indicates the angle between the propagating direction of the incident beam and the optics axis of the crystal. The spectral auto-convolution (solid white lines) [29] of the pulse, which is the desired second-harmonic spectrum of the pulse, is calculated by Eq. (2) ($\tau = 0$) and displayed in Fig. 1. When the phase-matching wavelength of a thick nonlinear crystal is within the spectral range of the measured pulse [the phase-matching wavelength at 32° (36°) is 732 nm (660 nm)], the frequency components near the phase-matching wavelength are much more efficient than other frequency components, resulting in a much narrower spectrum being observed as shown in Figs. 1(a) and 1(b). Nonetheless, the efficiency of each frequency component of the measured pulse is comparable when the phase-matching wavelength is tuned outside of the spectrum range (the phase-matching wavelength at 40° is 600 nm). As a result, the spectral width of the second harmonic remains almost unchanged for different BBO thicknesses as shown in Fig. 1(c). It shows that, under the phase-mismatching configuration,

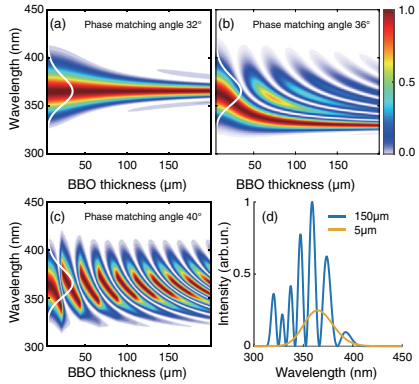

Fig. 1. Spectrum of the second harmonic generated by an 8 fs 730 nm Gaussian laser pulse with the increase of BBO thickness at different phase-matching angles (a) 32°, (b) 36°, (c) 40°. The white Gaussian curves represent the spectral auto-convolution of the laser pulse. The relative second-harmonic spectral intensity curves of the 37.6° 150 μm (blue) and 5 μm (gray) BBOs for the pulse are shown in (d).

the spectral auto-convolution width is comparable to that of the second-harmonic spectrum. This indicates that the phase-mismatching configuration can be applied to the measurement of ultrashort laser pulses even when a thick nonlinear crystal is used. Meanwhile, Fig. 1(d) shows the relative second-harmonic spectral intensity curves, calculated by Eqs. (1)–(3) ($\tau = 0$), of the 150 μm (blue) and 5 μm (gray) BBOs at 37.6° for the pulse. It is distinct that the 150 μm BBO does improve the conversion efficiency by a factor of 4 as compared to that of the 5 μm BBO.

The problem with applying this scheme to the measurement of ultrashort pulses is that the measured second-harmonic spectrum is modulated by the sinc^2 function in Eq. (3) [34]. As we can see from Fig. 1(b), with the angle of the nonlinear crystal deviating from the phase-matching angle for the central wavelength of the fundamental pulse, the modulation of the second-harmonic spectrum is obvious. It is thus important to confirm whether such modulated second-harmonic spectrum can be applied to a retrieving algorithm, such as the principal components generalized projections algorithm (PCGPA) [22], to extract the correct phase information.

In a real experiment, the detection device (spectrometer, CCD) has a finite dynamic range and inevitable thermal noise. When the intensity variation of the second harmonic across the spectral range surpasses the dynamic range of the detector, this correction method will fail to recover the ideal FROG trace because the signals with low efficiency will be buried under the thermal noise. To demonstrate the generality of the proposed method, we simulated a SHG-FROG trace by passing an 8.2 fs 700 nm complex pulse through a 40° 100 μm BBO using Eqs. (1)–(3). In the calculated trace, we considered 20 dB thermal noise on the detector and 14.5 meV frequency resolution of the spectrometer to mimic the experimental conditions. The calculated trace after spectral auto-convolution correction aforementioned is presented in Fig. 2(a). It can be seen that the overall FROG trace has been modulated along the energy axis (dotted lines) due to spectral filtering function [Eq. (3)]. However, by using a PCGPA, a smooth trace [Fig. 2(b)] that is very similar to the ideal trace [Fig. 2(c)] calculated by Eq. (2) can still be well retrieved. The FROG error is 0.77% (for a 1024 × 1024

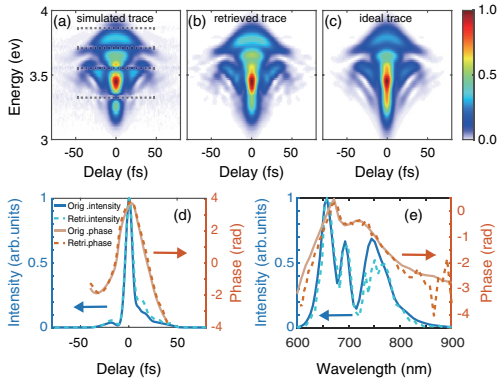

Fig. 2. (a) SHG-FROG trace calculated with an 8.2 fs 700 nm complex pulse through a 40° 100 μm BBO. Dotted lines represent the modulations by spectral filtering function [Eq. (3)]. (b) Reconstructed SHG-FROG trace retrieved from (a) using PCGPA. (c) Ideal SHG-FROG trace of the complex pulse calculated by Eq. (2). (d) Time domain intensity (blue dotted) and phase (orange dotted) of the retrieved pulse overlaid with the time domain intensity (dark blue solid) and phase (gray solid) of the original input pulse. (e) Similar to (d), but for the spectral intensity and phase of the short pulse.

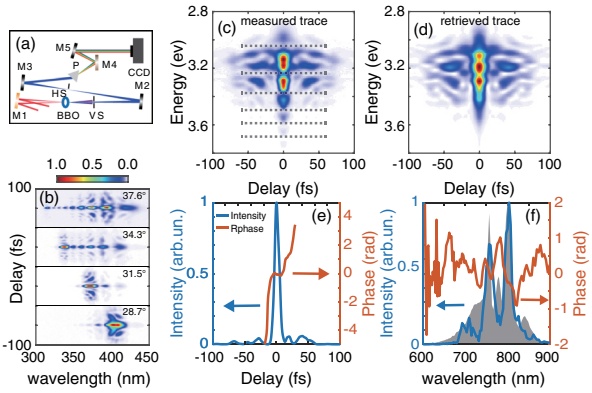

Fig. 3. (a) Experimental layout: M1, cylindrical mirror; VS, vertical slit; M2, M3, M5, ultraviolet (UV) concave mirror; M4, UV mirror; HS, horizontal slit; P, prism. (b) SHG-FROG trace measured at different phase-matching angles of 37.6°, 34.3°, 31.5°, and 28.7° from top to bottom using a 150 μm BBO. (c) Measured SHG-FROG trace using a 150 μm BBO at a phase-matching angle of 37.6°. Dotted lines represent the modulations by spectral filtering function [Eq. (3)]. (d) Reconstructed SHG-FROG trace from (c) using PCGPA. (e) Retrieved time domain intensity (blue solid) and phase (orange solid) of the short pulse. (f) Retrieved spectral intensity (blue solid) and phase (orange solid) of the short pulse, and the shaded area represents the spectral intensity of the pulse measured by the spectrometer.

matrix). The time (frequency) domain intensity and phase information of the retrieved pulse as compared to those of the original input pulse are shown in Fig. 2(d) [Fig. 2(e)]. Although it shows small discrepancy in the intensity profile due to the existence of the modulation, the phase information of the pulse, which is more crucial, is well recovered. Accompanied by a real spectrum measured using a standard optical spectrometer, the waveform of the ultrashort pulse can be completely determined. Similarly, we have performed simulations for larger phase-matching angles and different pulse parameters, and the reconstructed results are similar to Fig. 2, indicating the robustness of our method. The good agreement between the reconstructed and original pulses verifies the feasibility of this scheme for ultrashort pulse measurement.

It is worth mentioning that the ptychographic reconstruction algorithm demonstrated in [27] does a good job for reconstructing SHG-FROG traces with heave shape modulations including those influenced by phase-matching spectral filtering function, and therefore it can be a reliable alternative for retrieving the pulse information from the trace in Fig. 2(a).

In the experiment, a Ti:sapphire amplifier generates a 0.2 mJ 25 fs 800 nm near-infrared (NIR) laser pulse. We send the laser pulse through a 1 m hollow core fiber filled with 0.6 atm Ar, and extend the spectrum of the laser pulse to 600–900 nm. Then we compress the pulse by using broadband chirped mirrors and wedge pair. The compressed pulse is characterized using a home-built single-shot SHG-FROG device similar to [35]. The schematic illustration of the setup is shown in Fig. 3(a). The pulse to be measured is divided into two beams by the beam splitter, then both beams are focused on the BBO by a cylindrical mirror. The phase-matched second-harmonic signal is imaged on the CCD camera via two slits and a prism-based spectrometer calibrated by a mercury lamp.

To verify our method experimentally, we applied a 150 μm BBO crystal to characterize a few-cycle short pulse. Figure 3(b) shows the SHG-FROG traces for different angles of the optics axis. For angles of 37.6°, 34.3°, 31.5°, and 28.7°, the corresponding phase-matching wavelengths are 636 nm, 688 nm, 743 nm, and 813 nm, respectively. It shows that the spectral width of the complete trace is gradually recovered as the phase-matching angle increases, corresponding to the phase-matching wavelength gradually turning away from the spectral window of the measured pulse. This experimental observation is consistent with the predictions as shown in the simulated results of Fig. 1. When the phase-matching angle is increased to 37.6°, the spectrum of the second harmonic spans from 300–450 nm, which has covered the whole spectral range of the fundamental pulse (600–900 nm) to be measured. Therefore, we used the trace measured at an angle of 37.6° to extract the phase of the pulse using a retrieving algorithm. The measured trace corrected by the spectral auto-convolution function is shown in Fig. 3(c). Figure 3(d) shows the trace retrieved from Fig. 3(c). We can see that there are some structural differences between the measured and retrieved trace, which is similar to the simulation as shown in Fig. 2, and the FROG error is 0.81%. The reconstructed intensity and phase information are displayed in Figs. 3(e) and 3(f). The blue and orange lines represent the intensity and phase of the reconstructed pulse, respectively, while the shaded area represents the spectral intensity of the pulse measured by the spectrometer. The reconstructed spectral intensity of the pulse is relatively consistent with the measured one in Fig. 3(f), and the full width at half-maximum (FWHM) of the pulse is measured to be 8.6 fs as shown in Fig. 3(e). So far, we have demonstrated the measurement of a few-cycle pulse using a 150 μm BBO under phase-mismatching configuration.

In order to further verify the accuracy of the measurement results in Fig. 3, we used a 5 μm thin BBO with an angle of 35°, which has sufficient phase-matching bandwidth, to re-measure the few-cycle broadband pulse [29]. Similarly, the measured FROG trace corrected by the spectral auto-convolution function is used for pulse reconstruction. Figure 4 shows the comparison of the reconstructed results using a 5 μm BBO

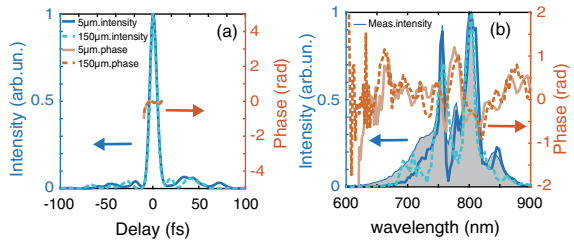

Fig. 4. Comparison of the short pulse retrieval using two BBOs with different thicknesses. (a) Retrieved time domain intensity (dark blue solid, blue dotted) and phase (gray solid, orange dotted) of the few-cycle pulse. (b) Similar to (a), but for the spectral intensity and phase of the short pulse. The shaded area represents the spectral intensity of the pulse measured by the spectrometer.

and a 150 μm BBO. The FROG error for the 5 μm BBO is 0.38%. The time domain intensity and phase information of the short pulse from both crystals show rather good agreement in Fig. 4(a), even though small discrepancy exists for the long-lasting pedestal of the pulses. The FWHM of the pulse is measured to be 9 fs using the 5 μm BBO, which is very close to 8.6 fs that is obtained from the thick BBO measurement. The retrieved phase from both BBOs are highly consistent as shown in Fig. 4(b). Similar to the results in Fig. 2, due to the sinc^2 modulation function along the energy axis, there is a slight deviation between the reconstructed and measured spectral intensity; however, the accurate retrieval of the spectral phase is more crucial for complete pulse characterization since the spectral intensity can be accurately detected using a standard spectrometer [36,37]. Consequently, the accuracy and feasibility of our scheme are verified experimentally. It is worth noticing that when an ultrashort pulse propagates through a nonlinear crystal with a thickness on the order of 100 μm, the pulse might be slightly elongated by the pulse propagation process in Eq. (3) (terms in brackets and Δk), causing an error of the measurement on the order of a few percent. Such effect can be reduced if the pulse to be measured is properly pre-compensated before interacting with the nonlinear crystal.

In conclusion, we have proposed and demonstrated a simple and efficient technique that allows both fast measurement of FROG trace and retrieval of the phase of an ultra-broadband laser pulse using a thick nonlinear crystal. The feasibility of this scheme is verified both theoretically and experimentally. We measured an ultrashort laser pulse of 8.6 fs with a 150 μm BBO in experiment, which agreed with the measurement results of a 5 μm BBO that support sufficient phase-matching bandwidth. This scheme not only reduces the requirement of nonlinear crystal for ultrashort laser pulse diagnosing, but it also improves the nonlinear efficiency. It circumvents the inherent shortcomings of the existing methods for ultrashort pulse measurement and will have a great application prospect.

Funding. National Key Research and Development Program of China (2017YFE0116600); National Natural Science Foundation of China (11774111, 12021004); International Cooperation program of the Hubei Innovation Fund (2019AHB052).

Disclosures. The authors declare no conflicts of interest.

REFERENCES

1. C. P. Hauri, W. Kornelis, F. W. Helbing, A. Heinrich, A. Couairon, A. Mysyrowicz, J. Biegert, and U. Keller, Appl. Phys. B **79**, 673 (2004).
2. A. Zaïr, A. Guandalini, F. Schapper, M. Holler, J. Biegert, L. Gallmann, A. Couairon, M. Franco, A. Mysyrowicz, and U. Keller, Opt. Express **15**, 5394 (2007).
3. A. Couairon, M. Franco, A. Mysyrowicz, J. Biegert, and U. Keller, Opt. Lett. **30**, 2657 (2005).
4. H. S. Chakraborty, M. B. Gaarde, and A. Couairon, Opt. Lett. **31**, 3662 (2006).
5. B. Schenkel, J. Biegert, U. Keller, C. Vozzi, M. Nisoli, G. Sansone, S. Stagira, S. D. Silvestri, and O. Svelto, Opt. Lett. **28**, 1987 (2003).
6. M. Nisoli, S. D. Silvestri, O. Svelto, R. Szipöcs, K. Ferencz, C. Spielmann, S. Sartania, and F. Krausz, Opt. Lett. **22**, 522 (1997).
7. M. Y. Shverdin, D. R. Walker, D. D. Yavuz, G. Y. Yin, and S. E. Harris, Phys. Rev. Lett. **94**, 033904 (2005).
8. T. Brabec and F. Krausz, Rev. Mod. Phys. **72**, 545 (2000).
9. N. Dudovich, O. Smirnova, J. Levesque, Y. Mairesse, M. Y. Ivanov, D. M. Villeneuve, and P. B. Corkum, Nat. Phys. **2**, 781 (2006).
10. F. Krausz and M. Ivanov, Rev. Mod. Phys. **81**, 163 (2009).
11. C. Ott, A. Kaldun, L. Argenti, P. Raith, K. Meyer, M. Laux, Y. Zhang, A. Blättermann, S. Hagstotz, T. Ding, R. Heck, J. Madroñero, F. Martín, and T. Pfeifer, Nature **516**, 374 (2014).
12. M. Nisoli, P. Decleva, F. Calegari, A. Palacios, and F. Martín, Chem. Rev. **117**, 10760 (2017).
13. F. Salin, P. Georges, G. Roger, and A. Brun, Appl. Opt. **26**, 4528 (1987).
14. J.-H. Chung and A. M. Weiner, IEEE J. Sel. Top. Quantum Electron. **7**, 656 (2001).
15. R. Trebino, K. W. DeLong, D. N. Fittinghoff, J. N. Sweetser, M. A. Krumbügel, B. A. Richman, and D. J. Kane, Rev. Sci. Instrum. **68**, 3277 (1997).
16. A. Baltuška, M. S. Pshenichnikov, and D. A. Wiersma, Opt. Lett. **23**, 1474 (1998).
17. D. J. Kane and R. Trebino, IEEE J. Quantum Electron. **29**, 571 (1993).
18. C. Iaconis and I. A. Walmsley, Opt. Lett. **23**, 792 (1998).
19. L. Gallmann, G. Steinmeyer, D. H. Sutter, T. Rupp, C. Iaconis, I. A. Walmsley, and U. Keller, Opt. Lett. **26**, 96 (2001).
20. M. Miranda, T. Fordell, C. Arnold, A. L'Huillier, and H. Crespo, Opt. Express **20**, 688 (2012).
21. M. Miranda, C. L. Arnold, T. Fordell, F. Silva, B. Alonso, R. Weigand, A. L'Huillier, and H. Crespo, Opt. Express **20**, 18732 (2012).
22. K. W. DeLong, D. N. Fittinghoff, R. Trebino, B. Kohler, and K. Wilson, Opt. Lett. **19**, 2152 (1994).
23. D. J. Kane, IEEE J. Sel. Top. Quantum Electron. **4**, 278 (1998).
24. K. W. DeLong and R. Trebino, J. Opt. Soc. Am. A **11**, 2429 (1994).
25. J. A. Nelder and R. Mead, Comput. J. **7**, 308 (1965).
26. T. Witting, F. Frank, C. A. Arrell, W. A. Okell, J. P. Marangos, and J. W. G. Tisch, Opt. Lett. **36**, 1680 (2011).
27. P. Sidorenko, O. Lahav, Z. Avnat, and O. Cohen, Optica **3**, 1320 (2016).
28. A. Baltuska, M. S. Pshenichnikov, and D. A. Wiersma, IEEE J. Quantum Electron. **35**, 459 (1999).
29. G. Taft, A. Rundquist, M. M. Murnane, I. P. Christov, H. C. Kapteyn, K. W. DeLong, D. N. Fittinghoff, M. A. Krumbugel, J. N. Sweetser, and R. Trebino, IEEE J. Sel. Top. Quantum Electron. **2**, 575 (1996).
30. P. O'Shea, M. Kimmel, X. Gu, and R. Trebino, Opt. Express **7**, 342 (2000).
31. C. Janisch, N. Mehta, D. Ma, A. L. Elías, N. Perea-López, M. Terrones, and Z. Liu, Opt. Lett. **39**, 383 (2014).
32. K. W. DeLong, R. Trebino, and D. J. Kane, J. Opt. Soc. Am. B **11**, 1595 (1994).
33. K. W. DeLong, D. N. Fittinghoff, and R. Trebino, IEEE J. Quantum Electron. **32**, 1253 (1996).
34. A. Weiner, IEEE J. Quantum Electron. **19**, 1276 (1983).
35. S. Akturk, C. D'Amico, and A. Mysyrowicz, J. Opt. Soc. Am. B **25**, A63 (2008).
36. H. Timmers, Y. Kobayashi, K. F. Chang, M. Reduzzi, D. M. Neumark, and S. R. Leone, Opt. Lett. **42**, 811 (2017).
37. F. Silva, B. Alonso, W. Holgado, R. Romero, J. S. Román, E. C. Jarque, H. Koop, V. Pervak, H. Crespo, I. Nigo, and J. Sola, Opt. Lett. **43**, 337 (2018).